



Neutron-star Radius Constraints from GW170817 and Future Detections

Andreas Bauswein¹, Oliver Just², Hans-Thomas Janka³, and Nikolaos Stergioulas⁴

¹Heidelberger Institut für Theoretische Studien, Schloss-Wolfsbrunnengasse 35, D-69118 Heidelberg, Germany; andreas.bauswein@h-its.org

²Astrophysical Big Bang Laboratory, RIKEN, Saitama 351-0198, Japan

³Max-Planck-Institut für Astrophysik, Karl-Schwarzschild-Str. 1, D-85748 Garching, Germany

⁴Department of Physics, Aristotle University of Thessaloniki, GR-54124 Thessaloniki, Greece

Received 2017 October 18; revised 2017 November 8; accepted 2017 November 8; published 2017 November 29

Abstract

We introduce a new, powerful method to constrain properties of neutron stars (NSs). We show that the total mass of GW170817 provides a reliable constraint on the stellar radius if the merger did not result in a prompt collapse as suggested by the interpretation of associated electromagnetic emission. The radius $R_{1.6}$ of nonrotating NSs with a mass of $1.6 M_{\odot}$ can be constrained to be larger than $10.68^{+0.15}_{-0.04}$ km, and the radius R_{\max} of the nonrotating maximum-mass configuration must be larger than $9.60^{+0.14}_{-0.03}$ km. We point out that detections of future events will further improve these constraints. Moreover, we show that a future event with a signature of a prompt collapse of the merger remnant will establish even stronger constraints on the NS radius from above and the maximum mass M_{\max} of NSs from above. These constraints are particularly robust because they only require a measurement of the chirp mass and a distinction between prompt and delayed collapse of the merger remnant, which may be inferred from the electromagnetic signal or even from the presence/absence of a ringdown gravitational-wave (GW) signal. This prospect strengthens the case of our novel method of constraining NS properties, which is directly applicable to future GW events with accompanying electromagnetic counterpart observations. We emphasize that this procedure is a new way of constraining NS radii from GW detections independent of existing efforts to infer radius information from the late inspiral phase or post-merger oscillations, and it does not require particularly loud GW events.

Key words: equation of state – gravitational waves – stars: neutron

1. Introduction

The recently detected GW170817 is the first observed gravitational-wave (GW) source involving matter (Abbott et al. 2017). The measured binary masses point to a merger of two neutron stars (NSs). Apart from the importance of this detection for stellar astrophysics and nucleosynthesis, such events are highly interesting because they bear the potential to infer weakly constrained properties of NSs (Lattimer & Prakash 2016; Özel & Freire 2016; Oertel et al. 2017). Such information can be obtained from the GW signal either from finite-size effects during the late inspiral phase (e.g., Faber et al. 2002; Flanagan & Hinderer 2008; Del Pozzo et al. 2013; Read et al. 2013; Abbott et al. 2017) or through the characteristic oscillations of the post-merger remnant (Bauswein & Janka 2012; Bauswein et al. 2012, 2014; Clark et al. 2014; Takami et al. 2014; Chatziioannou et al. 2017). Both approaches require high signal-to-noise ratios (S/Ns).

The merging of two NSs can result either in the direct formation of a black hole (BH) on a dynamical timescale (prompt collapse) or the formation of an at least transiently stable NS merger remnant (delayed/no collapse). The former case occurs for mergers with binary masses M_{tot} above a threshold binary mass M_{thres} , a delayed, or no, collapse results for binaries with $M_{\text{tot}} < M_{\text{thres}}$. The two different collapse scenarios are also expected to lead to different electromagnetic emission. The amount of dynamical ejecta is strongly reduced in the case of prompt BH formation (Bauswein et al. 2013b; Hotokezaka et al. 2013). Also, the different nature of the merger remnant yields different amounts of secular ejecta (Fernández & Metzger 2013; Metzger & Fernández 2014; Perego et al. 2014; Siegel et al. 2014; Just et al. 2015).

In this Letter, we present a new method to infer information on the NS equation of state (EoS) from NS mergers that does

not require a high S/N of the GW measurement. Our constraint only relies on the measured binary mass of GW170817 and the evidence for a delayed/no collapse in this event as suggested by its electromagnetic emission (e.g., Kasen et al. 2017; Metzger 2017). In the case of a delayed/no collapse, the measured total binary mass of GW170817 provides a lower bound on the threshold mass for direct BH formation,

$$M_{\text{thres}} > M_{\text{tot}}^{\text{GW170817}} = 2.74^{+0.04}_{-0.01} M_{\odot}, \quad (1)$$

and we conclude that the radius $R_{1.6}$ of a NS with $1.6 M_{\odot}$ must be larger than $10.68^{+0.15}_{-0.04}$ km. We demonstrate that our new method promises very strong constraints on NS radii and the maximum mass M_{\max} of nonrotating NSs if more NS mergers are observed and in particular if an event with a prompt collapse of the merger remnant is identified.

2. Observations

Several telescopes observed emission in the X-ray, optical, and infrared from the GW source with spatial and temporal coincidence (LIGO Scientific Collaboration et al. 2017). The observations are compatible with NS merger ejecta that are heated by the nuclear decays of products of the rapid neutron-capture process (Metzger et al. 2010). The light-curve properties were interpreted as being produced by dynamical ejecta from the merger and secular ejecta from the merger remnant. The estimated ejecta mass is in the range of 0.03 to 0.05 M_{\odot} (Chornock et al. 2017; Cowperthwaite et al. 2017; Drout et al. 2017; Kasen et al. 2017; Kasliwal et al. 2017; Kilpatrick et al. 2017; Nicholl et al. 2017; Smartt et al. 2017; Tanaka et al. 2017; Tanvir et al. 2017), which even for asymmetric binaries lies near the high end of the theoretical range expected from simulations. This can be

interpreted as tentative evidence for a delayed/no collapse in GW170817 because this merger outcome tends to produce larger ejecta masses as compared to a direct collapse (Bauswein et al. 2013b; Fernández & Metzger 2013; Hotokezaka et al. 2013; Metzger & Fernández 2014; Perego et al. 2014; Siegel et al. 2014; Wanajo et al. 2014; Just et al. 2015; Sekiguchi et al. 2016). We thus use below the assumption of no prompt collapse in GW170817 and leave the detailed interpretation of the electromagnetic emission to future work. Our assumption can be corroborated by refined models and future observations.

3. NS Radius Constraints

3.1. Threshold Binary Mass

If GW170817 resulted in a delayed collapse or no collapse, its total mass provides a lower limit on the threshold binary mass for prompt collapse as given by Equation (1).

The threshold binary mass M_{thres} depends sensitively on the EoS (Shibata 2005; Baiotti et al. 2008; Hotokezaka et al. 2011; Bauswein et al. 2013a). Considering different EoSs, in Bauswein et al. (2013a), we found by hydrodynamical simulations that the threshold binary mass to good accuracy follows

$$M_{\text{thres}} = \left(-3.606 \frac{GM_{\text{max}}}{c^2 R_{1.6}} + 2.38 \right) \cdot M_{\text{max}} \quad (2)$$

with $R_{1.6}$ being the radius of a nonrotating NS with a mass of $1.6 M_{\odot}$ and M_{max} being the maximum mass of nonrotating NSs. The relation was derived from simulations of symmetric binary mergers but also holds for moderately asymmetric systems (Bauswein et al. 2013a; Bauswein & Stergioulas 2017). We verify through additional simulations for five representative EoSs that strongly asymmetric mergers with mass ratio $q = 0.6$ have a threshold binary mass, which is systematically lower by 0.1 to $0.3 M_{\odot}$ than M_{thres} of equal-mass binaries. This reduction of M_{thres} for asymmetric binaries is understandable because, according to *Kepler's* law, asymmetric binaries have less angular momentum than equal-mass binaries with the same M_{tot} at a given orbital separation, which implies less stabilization for asymmetric mergers. (With the low-spin priors, the 90% credibility interval of the mass ratio of GW170817 is $q = 0.7\text{--}1.0$). If GW170817 was very asymmetric, one has $M_{\text{thres}}^{\text{asym}} \geq M_{\text{tot}}$, which implies that Equation (1) is conservative because $M_{\text{thres}} > M_{\text{thres}}^{\text{asym}}$.

A similarly accurate description of M_{thres} is given by the fit

$$M_{\text{thres}} = \left(-3.38 \frac{GM_{\text{max}}}{c^2 R_{\text{max}}} + 2.43 \right) \cdot M_{\text{max}}, \quad (3)$$

with the radius R_{max} of the maximum-mass configuration. Equation (2) is accurate to better than $0.1 M_{\odot}$ (Bauswein et al. 2013a, 2016). The existence of these relations has been solidified by semi-analytic calculations of equilibrium models (Bauswein & Stergioulas 2017).

3.2. Radius Constraints

Equations (2) and (3) imply constraints on NS radii $R_{1.6}$ and R_{max} since the total binary mass of GW170817 represents a lower bound on M_{thres} (Equation (1)). Figure 1 (left panel) shows $M_{\text{thres}}(M_{\text{max}}; R_{1.6})$ (Equation (2)) for different chosen

values of $R_{1.6}$ (solid lines). Every sequence terminates at

$$M_{\text{max}} = \frac{1}{3.10} \frac{c^2 R_{1.6}}{G}, \quad (4)$$

which is an empirical upper limit on M_{max} for the given $R_{1.6}$. Extending various microphysical EoSs with a maximally stiff EoS, i.e., $v_{\text{sound}} = c$, beyond the central density of an NS with $1.6 M_{\odot}$ determines the highest possible M_{max} for a given $R_{1.6}$ compatible with causality. With Equation (2), it implies $M_{\text{thres}} \geq 1.22 M_{\text{max}}$.

In Figure 1 the horizontal dark blue band refers to the measured lower limit of M_{thres} given by the total binary mass of GW170817 (Equation (1)). This GW measurement thus rules out EoSs with very small $R_{1.6}$ because those EoSs would not result in a delayed collapse for the measured binary mass. The allowed range of possible stellar parameters is indicated by the light blue area. The solid blue curve corresponds to the smallest $R_{1.6}$ compatible with Equation (1). Hence, the radius of a $1.6 M_{\odot}$ NS must be larger than $10.30^{+0.15}_{-0.03}$ km. The error bar corresponds to the radii compatible with the error in M_{tot} . Arguments about the error budget and the robustness are provided in Section 3.3.

Figure 1 (right panel) displays $M_{\text{thres}}(M_{\text{max}}; R_{\text{max}})$ for different chosen R_{max} (solid lines). The different sequences for fixed R_{max} are constrained by causality (Koranda et al. 1997; Lattimer & Prakash 2016), requiring

$$M_{\text{max}} \leq \frac{1}{2.82} \frac{c^2 R_{\text{max}}}{G} \quad (5)$$

and with Equation (3)

$$M_{\text{thres}} \geq 1.23 M_{\text{max}}. \quad (6)$$

The lower bound of M_{thres} given by the measured total mass of GW170817 is shown as a dark blue band. The radius R_{max} of the nonrotating maximum-mass NS is thus constrained to be larger than $9.26^{+0.17}_{-0.03}$ km.

Instead of using Equation (1), it may be more realistic to assume that the remnant was stable for at least 10 ms to yield the observed ejecta properties (high masses, blue component) (Cowperthwaite et al. 2017; Margalit & Metzger 2017; Nicholl et al. 2017). In this case, our numerical simulations suggest that $M_{\text{thres}} - M_{\text{tot}} \geq 0.1 M_{\odot}$. This strengthens the radius constraints to $R_{1.6} \geq 10.68^{+0.15}_{-0.04}$ km and $R_{\text{max}} \geq 9.60^{+0.14}_{-0.03}$ km.

Figure 2 shows these radius constraints overlaid on mass-radius relations of different EoSs available in the literature. Our new radius constraints for $R_{1.6}$ and R_{max} derived from GW170817 exclude EoS models describing very soft nuclear matter. For the three EoSs excluded by our “realistic” constraint in Figure 2, e.g., the softest EoS in Hebeler et al. (2013), we cross-checked that numerical simulations with the binary masses of GW170817 do indeed result in a prompt collapse.

3.3. Discussion: Robustness and Errors

We took an overall conservative approach in this first study. Future refinements may strengthen these constraints. Our way of inferring NS radii is particularly appealing and robust because it only relies on (1) a well measured quantity (total binary mass with reliable error bars), (2) a single verifiable empirical relation (Equation (2) or (3)) derived from simulations, and (3) a clearly defined working hypothesis (delayed/no collapse of the merger remnant). All assumptions can be further substantiated and refined

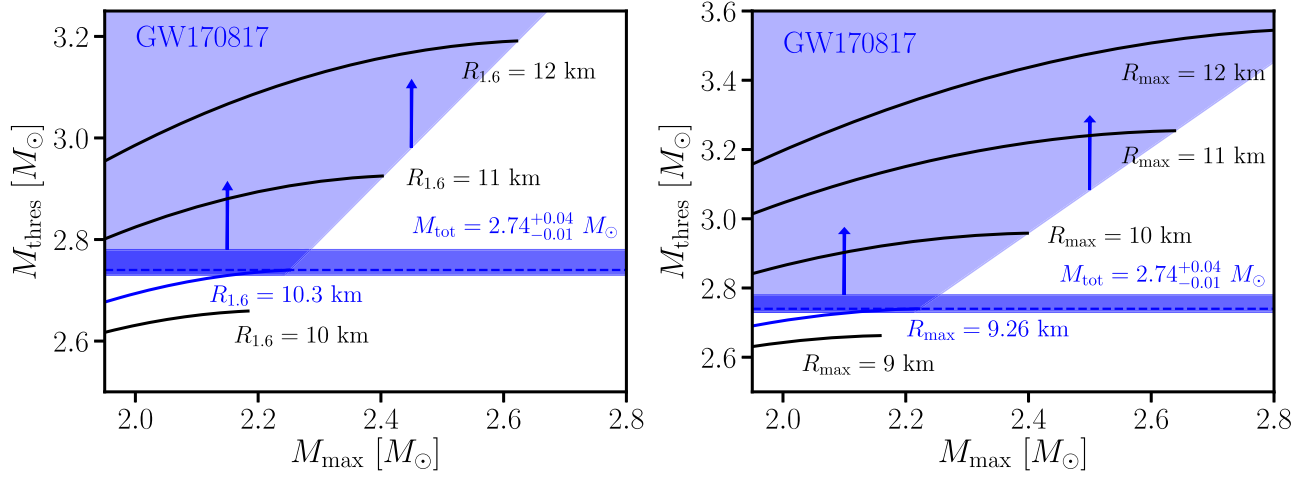


Figure 1. Threshold binary mass M_{thres} for prompt collapse as a function of M_{max} for different $R_{1.6}$ (left panel, Equation (2)) and R_{max} (right panel, Equation (3); solid lines). The dark blue band shows the total binary mass of GW170817, providing a lower limit on M_{thres} . The true M_{thres} must lie within the light blue areas if GW170817 resulted in a delayed/no collapse. This rules out NSs with $R_{1.6} \leq 10.30^{+0.18}_{-0.03}$ km and $R_{\text{max}} \leq 9.26^{+0.17}_{-0.03}$ km. Causality requires $M_{\text{thres}} \geq 1.22M_{\text{max}}$ (left panel) and $M_{\text{thres}} \geq 1.23M_{\text{max}}$ (right panel).

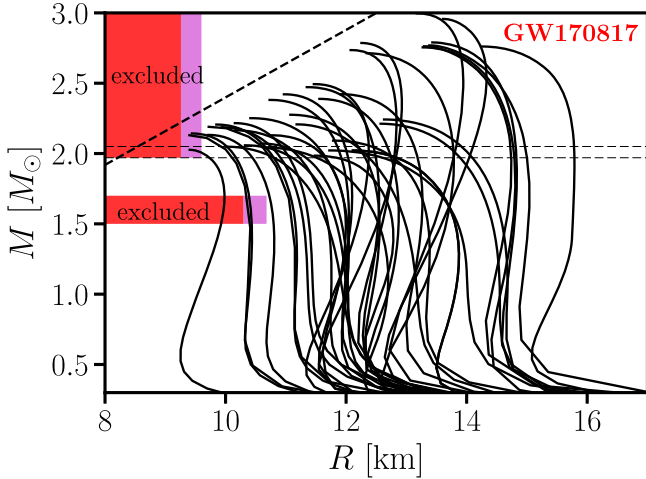


Figure 2. Mass–radius relations of different EoSs with very conservative (red area) and “realistic” (cyan area) constraints of this work for $R_{1.6}$ and R_{max} . Horizontal lines display the limit by Antoniadis et al. (2013). The dashed line shows the causality limit.

by more advanced models and future observations, and error bars can be robustly quantified.

(1) Mass measurement: The total binary mass can be measured with good accuracy and the error bars are given with high confidence. We fully propagate the error through our analysis using the low-spin prior results of Abbott et al. (2017). If GW170817 was an asymmetric merger as tentatively suggested by the high ejecta mass, the true M_{tot} lies at the upper bound of the error band and our radius constraints become stronger.

(2) Accuracy of empirical relations for M_{thres} : The empirical relations (Equations (2) and (3)) are inferred from hydrodynamical simulations (Bauswein et al. 2013a, 2016) and carry a systematic error⁵ and an intrinsic scatter (stemming from the sample of candidate EoSs, which do not perfectly fulfill the

⁵ Simulations for determining M_{thres} and corresponding fits employ a conformally flat spatial metric with a GW backreaction scheme (Oechslin et al. 2007; Bauswein et al. 2013a), which results in a slightly decelerated inspiral (compared to fully relativistic calculations) and thus leads to a slight overestimation of M_{thres} by $\sim 0.05 M_{\odot}$. We will quantify this effect in future work and emphasize that a small overestimation implies that our radius constraints are conservative.

analytic fit). M_{thres} has been numerically determined with a precision of $\pm 0.05 M_{\odot}$. Deviations between fits and numerical data are on average less than $0.03 M_{\odot}$ and at most $0.075 M_{\odot}$.⁶ We do not include this uncertainty in our error analysis because the numerically determined M_{thres} of all tested microphysical candidate EoSs is significantly smaller than the maximum of the $M_{\text{thres}}(M_{\text{max}})$ sequence for the radius given by the respective EoS.⁷ Recall that the maxima of the $M_{\text{thres}}(M_{\text{max}})$ sequences are given by maximally (unrealistically) stiff EoSs only constrained by causality. We thus remain conservative by determining minimum NS radii through the maxima of the sequences defined by causality.

We note that evidence for a long-lived merger remnant (e.g., Lippuner et al. 2017; Margalit & Metzger 2017) further strengthens our arguments. The longer the remnant lifetime τ , the larger the difference $M_{\text{thres}} - M_{\text{tot}} > 0$, which implies stronger radius constraints (see above). These considerations emphasize the importance of a better understanding of the dependence of the remnant lifetime on the binary mass, which represents a challenge for numerical simulations, but could yield even stronger radius constraints (see Section 4). Currently, the lifetime of presumably more than just a few milliseconds for the remnant in GW170817 implies an additional buffer in our error analysis.

The validity of Equations (2) and (3) and their uncertainties should be explored by future simulations employing an even larger set of EoSs (including models of absolutely stable quark matter) and successively improved numerical modeling.

Obviously, the merger outcome for a given EoS can be directly tested through numerical simulations for the measured binary masses to validate our constraints.

⁶ We computed M_{thres} for six additional EoSs not included in Bauswein et al. (2013a) to verify this accuracy, in particular, for EoS models yielding relatively small NS radii (as small as $R_{1.6} = 10.37$ km).

⁷ Within our sample of 17 candidate EoSs, the true M_{thres} is on average $0.17 M_{\odot}$ ($0.14 M_{\odot}$ for the R_{max} sequence) below the maximum $M_{\text{thres}}^{\text{up}}$ of the $M_{\text{thres}}(M_{\text{max}}, R)$ relation, which well justifies the neglect of the scatter in Equations (2) and (3). Three EoSs (eosAU, WFF1, and LS375) are relatively close to the maximum ($\sim 0.02 M_{\odot}$ below $M_{\text{thres}}^{\text{up}}$). However, these EoS models become acausal ($v_{\text{sound}} > c$), i.e., unrealistically stiff, at densities of high-mass merger remnants, which artificially increases M_{thres} . For these EoSs, we determined M_{thres} with a precision of $\pm 0.025 M_{\odot}$.

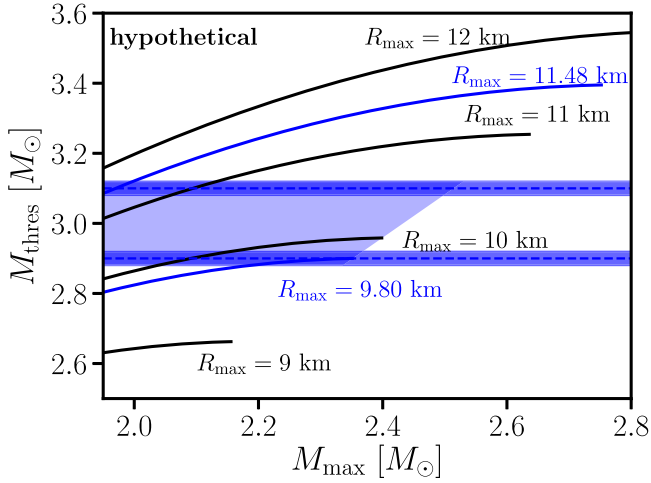


Figure 3. Same as Figure 1 (right panel). Dark blue bands display binary masses of hypothetical events with $2.9 M_{\odot}$ resulting in a delayed collapse and $3.1 M_{\odot}$ resulting in a prompt collapse. Viable NS properties are constrained to the light blue area.

(3) Distinction of collapse scenarios: The scenario of a delayed/no collapse in GW170817 can be consolidated by more advanced models of the electromagnetic emission. We anticipate that as more GW and counterpart observations become available in the future, the comprehension of their emission features will grow and will allow for a more robust distinction between prompt and delayed-collapse events. The growing understanding can be applied to the interpretation of past events by using additional information about the remnant lifetime for continuous refinements of the radius constraints. The interpretation of electromagnetic emission resulting from prompt or delayed collapse can be tested in the future also by measuring post-merger GW emission (Clark et al. 2014).

4. Future Measurements

Ideas introduced in this paper bear the potential of very strong EoS constraints as they are applied to future GW events with higher binary masses. We point out three future hypothetical scenarios.

(1) If an event with higher chirp mass than in GW170817 is detected and evidence for a delayed/no collapse is found, the lower bound on M_{thres} increases. The dark blue band in Figure 1 shifts to higher M_{thres} and NS radii must be larger than implied by GW170817. This is sketched in Figure 3 for a hypothetical event with $M_{\text{tot}} = (2.9 \pm 0.02) M_{\odot}$.

(2) If an event with a higher chirp mass than in GW170817 and a signature of a prompt collapse is observed, this will establish an upper bound on M_{thres} . Figure 3 shows this case for a hypothetical binary mass of $3.1 M_{\odot}$. This measurement would imply an upper bound on NS radii, here $R_{1.6} \leq 13$ km and $R_{\text{max}} \leq 11.48$ km, and an upper bound on M_{max} ($\sim 2.5 M_{\odot}$ for this hypothetical case). These limits are visualized in Figure 4. The upper right exclusion region is given by the solution to $M_{\text{tot}} = 3.1 M_{\odot} = (-3.38 \frac{GM_{\text{max}}}{c^2 R_{\text{max}}} + 2.43) M_{\text{max}}$ (Equation (3)). As more detections with different binary masses are made, M_{thres} will be constrained increasingly tighter from above and below. This will limit NS radii, i.e., R_{max} and $R_{1.6}$, and M_{max} to a relatively narrow range. M_{max} will be constrained from above and possibly determined

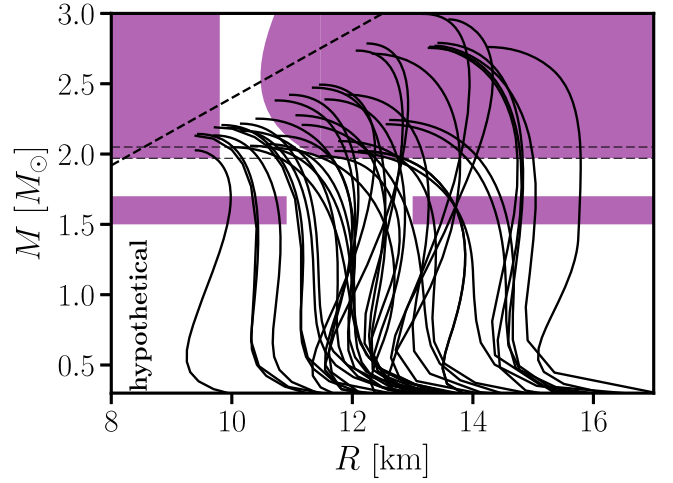


Figure 4. Mass–radius relations of different EoSs with hypothetical exclusion regions (purple areas) from a delayed-collapse event with $M_{\text{tot}} = 2.9 M_{\odot}$ and a prompt-collapse event with $M_{\text{tot}} = 3.1 M_{\odot}$ employing the methods of this work (compare to Figure 3).

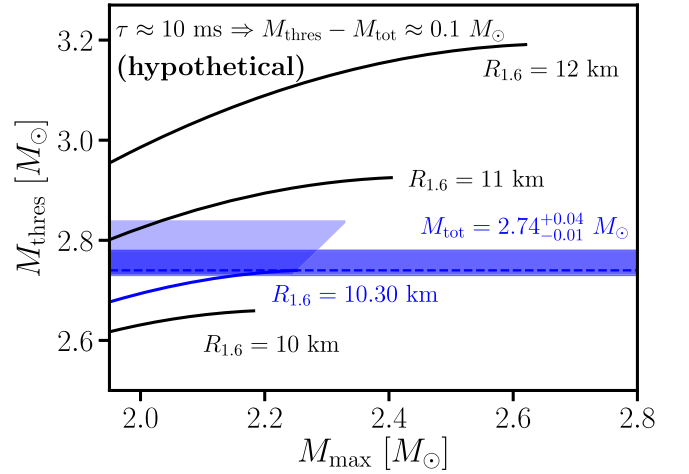


Figure 5. Same as Figure 1 (left panel), hypothetically assuming evidence for a remnant lifetime of $\tau \leq 10$ ms in an event like GW170817. NS properties $R_{1.6}$ and M_{max} would be constrained to the light blue area, implying tight bounds on $R_{1.6}$.

with good accuracy if NS radii can be narrowed down by other even more accurate methods.

(3) Events with an upper bound on the remnant lifetime effectively establish an upper bound on M_{thres} with similar implications as in the previous scenario. This requires a better understanding of the exact dependence of the lifetime on binary masses and a reliable way to constrain the lifetime from observations, both of which can be achieved through improved numerical or analytic models. We sketch a hypothetical case in Figure 5.

5. Conclusions

We introduce a new method to constrain NS radii and the maximum mass from GW observations of NS mergers and the observational distinction between a delayed and prompt collapse of the merger remnant. Based on the binary mass measurement of GW170817 and the well justified hypothesis

of a delayed/no collapse in this event (e.g., Margalit & Metzger 2017; Metzger 2017; Nicholl et al. 2017), we show that the radius of a $1.6 M_{\odot}$ NS must be larger than $10.68_{-0.04}^{+0.15}$ km and the radius of the maximum-mass configuration, R_{\max} , is larger than $9.60_{-0.03}^{+0.14}$ km. We stress the potential of future GW events. In particular, an event associated with a prompt collapse will constrain NS radii from above as well as the maximum mass M_{\max} of nonrotating NSs. As the sensitivity of GW detectors increases, more events with more accurate mass measurements can be expected. Similarly, we anticipate a more robust identification of the collapse behavior as more electromagnetic counterparts are observed and increasingly better understood theoretically.

Our new method is particularly promising because it does not require higher S/Ns of future GW events and is thus directly applicable to any new event within the era of current detectors for which the collapse behavior can be classified. It provides a robust, complimentary way of constraining the high-density EoS, independent of efforts to measure finite-size effects during the late inspiral phase (Faber et al. 2002; Flanagan & Hinderer 2008; Del Pozzo et al. 2013; Read et al. 2013; Abbott et al. 2017) or prospects to detect oscillations from the post-merger phase (Bauswein & Janka 2012; Bauswein et al. 2012, 2014; Clark et al. 2014; Chatziioannou et al. 2017). See, e.g., Lawrence et al. (2015), Fryer et al. (2015), Margalit & Metzger (2017) for alternative methods to constrain M_{\max} .

Apart from the model-dependent interpretation of the electromagnetic emission, our method only relies on binary mass measurements and empirical relations describing $M_{\text{thres}}(M_{\max}, R)$. Future calculations can further corroborate these relations for a larger sample of candidate EoSs and with more sophisticated models, although it seems unlikely that for instance a detailed incorporation of neutrinos or magnetic fields can have a significant influence on the relations for the threshold mass. We emphasize the simplicity and robustness of our constraints as a major advantage.

We demonstrated this robustness with the observation of GW170817 and its electromagnetic counterpart making conservative assumptions throughout, for instance, by assuming an equal-mass merger. Future work should refine this first study and will yield stronger radius constraints. Specifically, we refer to the inclusion of mass-ratio effects and additional information from limits on the remnant lifetime. As follow-up to this Letter, we will update our radius constraints following the methods described here as new measurements become available.⁸

We thank K. Hebeler for EoS tables. A.B. acknowledges support by the Klaus Tschira Foundation. Partial support comes from COST actions GWverse CA16104 and PHAROS CA16214 and from the DAAD Germany-Greece grant ID 57340132. H.-T.J. acknowledges support by the European Research Council through grant ERC AdG 341157-COCO2-CASA and by the Deutsche Forschungsgemeinschaft through grants SFB 1258 and EXC 153 and thanks the Mainz Institute for Theoretical Physics.

ORCID iDs

Andreas Bauswein  <https://orcid.org/0000-0001-6798-3572>
 Oliver Just  <https://orcid.org/0000-0002-3126-9913>
 Hans-Thomas Janka  <https://orcid.org/0000-0002-0831-3330>

References

- Abbott, B. P., Abbott, R., Abbott, T. D., et al. 2017, *PhRvL*, **119**, 161101
 Antoniadis, J., Freire, P. C. C., Wex, N., et al. 2013, *Sci*, **340**, 448
 Baiotti, L., Giacomazzo, B., & Rezzolla, L. 2008, *PhRvD*, **78**, 084033
 Bauswein, A., Baumgarte, T. W., & Janka, H.-T. 2013a, *PhRvL*, **111**, 131101
 Bauswein, A., Goriely, S., & Janka, H.-T. 2013b, *ApJ*, **773**, 78
 Bauswein, A., & Janka, H.-T. 2012, *PhRvL*, **108**, 011101
 Bauswein, A., Janka, H.-T., Hebeler, K., & Schwenk, A. 2012, *PhRvD*, **86**, 063001
 Bauswein, A., & Stergioulas, N. 2017, *MNRAS*, **471**, 4956
 Bauswein, A., Stergioulas, N., & Janka, H.-T. 2014, *PhRvD*, **90**, 023002
 Bauswein, A., Stergioulas, N., & Janka, H.-T. 2016, *EPJA*, **52**, 56
 Chatziioannou, K., Clark, J. A., Bauswein, A., et al. 2017, PhRvD, submitted (arXiv:1711.00040)
 Chornock, R., Berger, E., Kasen, D., et al. 2017, *ApJL*, **848**, L18
 Clark, J., Bauswein, A., Cadonati, L., et al. 2014, *PhRvD*, **90**, 062004
 Cowperthwaite, P. S., Berger, E., Villar, V. A., et al. 2017, *ApJL*, **848**, L17
 Del Pozzo, W., Li, T. G. F., Agathos, M., Van Den Broeck, C., & Vitale, S. 2013, *PhRvL*, **111**, 071101
 Drout, M. R., Piro, A. L., Shappee, B. J., et al. 2017, *Sci*, <https://doi.org/10.1126/science.aag0049>
 Faber, J. A., Grandclément, P., Rasio, F. A., & Taniguchi, K. 2002, *PhRvL*, **89**, 231102
 Fernández, R., & Metzger, B. D. 2013, *MNRAS*, **435**, 502
 Fryer, C. L., Belczynski, K., Ramirez-Ruiz, E., et al. 2015, *ApJ*, **812**, 24
 Hebeler, K., Lattimer, J. M., Pethick, C. J., & Schwenk, A. 2013, *ApJ*, **773**, 11
 Flanagan, É. É., & Hinderer, T. 2008, *PhRvD*, **77**, 021502
 Hotokezaka, K., Kiuchi, K., Kyutoku, K., et al. 2013, *PhRvD*, **87**, 024001
 Hotokezaka, K., Kyutoku, K., Okawa, H., Shibata, M., & Kiuchi, K. 2011, *PhRvD*, **83**, 124008
 Just, O., Bauswein, A., Pulpillo, R. A., Goriely, S., & Janka, H.-T. 2015, *MNRAS*, **448**, 541
 Kasen, D., Metzger, B., Barnes, J., Quataert, E., & Ramirez-Ruiz, E. 2017, *Natur*, **551**, 80
 Kasliwal, M. M., Nakar, E., Singer, L. P., et al. 2017, *Sci*, <https://doi.org/10.1126/science.aap9455>
 Kilpatrick, C. D., Foley, R. J., Kasen, D., et al. 2017, *Sci*, <https://doi.org/10.1126/science.aag0073>
 Koranda, S., Stergioulas, N., & Friedman, J. L. 1997, *ApJ*, **488**, 799
 Lattimer, J. M., & Prakash, M. 2016, *PhR*, **621**, 127
 Lawrence, S., Tervala, J. G., Bedaque, P. F., & Miller, M. C. 2015, *ApJ*, **808**, 186
 LIGO Scientific Collaboration, Virgo Collaboration et al. 2017, *ApJL*, **848**, L12
 Lippuner, J., Fernández, R., Roberts, L. F., et al. 2017, *MNRAS*, **472**, 904
 Margalit, B., & Metzger, B. 2017, *ApJL*, **850**, L19
 Metzger, B. D. 2017, arXiv:1710.05931v1
 Metzger, B. D., & Fernández, R. 2014, *MNRAS*, **441**, 3444
 Metzger, B. D., Martínez-Pinedo, G., Darbha, S., et al. 2010, *MNRAS*, **406**, 2650
 Nicholl, M., Berger, E., Kasen, D., et al. 2017, *ApJL*, **848**, L18
 Oechslin, R., Janka, H.-T., & Marek, A. 2007, *A&A*, **467**, 395
 Oertel, M., Hempel, M., Klähn, T., & Typel, S. 2017, *RvMP*, **89**, 015007
 Özel, F., & Freire, P. 2016, *ARA&A*, **54**, 401
 Perego, A., Rosswog, S., Cabezón, R. M., et al. 2014, *MNRAS*, **443**, 3134
 Read, J. S., Baiotti, L., Creighton, J. D. E., et al. 2013, *PhRvD*, **88**, 044042
 Sekiguchi, Y., Kiuchi, K., Kyutoku, K., Shibata, M., & Taniguchi, K. 2016, *PhRvD*, **93**, 124046
 Shibata, M. 2005, *PhRvL*, **94**, 201101
 Siegel, D. M., Ciolfi, R., & Rezzolla, L. 2014, *ApJL*, **785**, L6
 Smartt, S. J., Chen, T.-W., Jerkstrand, A., et al. 2017, *Natur*, **551**, 75
 Takami, K., Rezzolla, L., & Baiotti, L. 2014, *PhRvL*, **113**, 091104
 Tanaka, M., Utsumi, Y., Mazzali, P. A., et al. 2017, PASJ, in press (arXiv:1710.05850)
 Tanvir, N. R., Levan, A. J., Gonzalez-Fernandez, C., et al. 2017, *ApJL*, **848**, L27
 Wanajo, S., Sekiguchi, Y., Nishimura, N., et al. 2014, *ApJL*, **789**, L39

⁸ Updated constraints will be published on <http://wwwmpa.mpa-garching.mpg.de/~bauswein/radiusconstraint/>.